Taylor & Francis
Taylor & Francis Group

STRUCTURAL, OPTICAL AND ELECTROCHROMIC PROPERTIES OF SOL–GEL V_2O_5 THIN FILMS

M. BENMOUSSA*, A. OUTZOURHIT, R. JOURDANI, A. BENNOUNA
and E. L. AMEZIANE

Laboratoire de Physique des Solides et des Couches Minces, Faculté des Sciences Semlalia,
B.P. 2390, Marrakech, Morocco

Vanadium pentoxide thin films are prepared by the sol–gel route by dissolving V_2O_5 powder (99.5% purity) in H_2O_2 solution. The solution is spin-coated on glass substrates for optical (UV–VIS–NIR) and XRD analysis, and on ITO-coated glass substrates for electrochromic measurements. The samples are then annealed at $150\,°C$ for 1 hour. The resulting films have a yellow-orange color, typical of polycrystalline V_2O_5. XRD measurements have shown that after annealing in air at $400\,°C$ the structure of the films has a c-axis preferred orientation, the $(0\,0\,1)$-type planes lying parallel to the substrate. SEM analysis revealed a smooth surface. The films' optical and physical constants (n, α, Eg, the thickness d and the mean thickness inhomogeneity σ) are calculated using a simple and accurate method based on the transmission spectrum alone. The films' electrochromism is studied using cyclic voltammetry (CV) and chronoamperometry in propylene carbonate solution containing $1\,mol/l$ $LiClO_4$. The films show reversible multichromism (yellow–green–blue) upon Li^+ ion insertion/extraction. The absorbance of films colored at three different potentials is measured in the UV–VIS–PIR wavelength range, and this study shows that the changes in the optical absorption are consistent with the film color changes. Finally, the optical and electrochromic properties of the films prepared by this method are compared with those of our sputtered films already studied and with other works.

Keywords: Vanadium pentoxide; Sol–gel; Spin-coating; Electrochromism; Structural properties; Optical properties

1 INTRODUCTION

V_2O_5 crystallizes in a layered structure and serves as a host material for a wide variety of metal cations. In particular, the large lithium insertion capacity of V_2O_5 films makes them attractive for use in high-capacity lithium batteries and in electrochromic devices either as electrochromic electrodes or as passive lithium reservoirs [1, 2]. V_2O_5 has also been used in WO_3–V_2O_5 composite films to change the bright blue color of WO_3 in the reduced state which is not as suitable as neutral gray or bronze colors for most building applications. In the reduced state, the WO_3–V_2O_5 composite films have dark or light brownish-blue color depending on the amount of vanadium and tungsten oxides [3]. For some applications, microporous sol–gel thin films may be appropriate. V_2O_5 thin films have been prepared from gels using either spin-coating [3–6] or dip-coating [7–9] methods. The aim of this work is to present a

---

* Corresponding author. Tel.: +(212) 44 43 74 10; Fax: +(212) 44 43 74 10; E-mail: benmoussa@ucam.ac.ma

structural, optical and electrochromic study of V_2O_5 thin films prepared by sol–gel spin coating route. First, experimental details of the film growth are given. Then, the structure of the films annealed at different temperatures is illustrated using the XRD measurements. The refractive index n(λ), absorption coefficient $\alpha(\lambda)$, optical gap energy Eg and film thickness d, are calculated from transmission spectra using an accurate optical method [10]. Electrochromism of the films is also studied using CV and chronoamperometry. Finally, a comparison of these results with those of sputtered films [11, 12] and of other works is given.

2 EXPERIMENTAL DETAILS

V_2O_5 thin films were prepared by sol–gel spin coating method. 0.5 g V_2O_5 powder (99.5% purity) was dissolved in 30 ml of 15% H_2O_2 solution under vigorous agitation. The red-brownish solution obtained transformed into a viscous solution after heat treatment in a water-bath at 70 °C for 20 min. The viscosity of the gel was found to depend on the water-bath temperature and on the heating time. A small portion of the solution was spin-coated on glass or on an indium tin oxide (ITO)-coated glass substrate at a suitable speed of 1800 to 6000 rpm depending on the required film thickness. The samples were then annealed in air at 150 °C for 1 hour. The resulting films have a yellow-orange color, typical of polycrystalline V_2O_5. Diffraction patterns were obtained using the CuKα radiation (1.542 Å). The surface morphology of the films was examined using a JEOL model JSM 5500 scanning electron microscope (SEM). The electrochromic measurements were performed in a cell containing the V_2O_5 sample as a working electrode, a Pt counter electrode, a Saturated Calomel Electrode (SCE) and a 1 M LiClO$_4$/propylene carbonate (PC) electrolyte. A bridge containing the PC electrolyte was used to separate the SCE from the electrolyte in the sample compartment. Standard procedure was followed in the preparation of the solutions, which were prepared in the presence of a silica gel to minimize water uptake of the salt and electrolyte. An EG&G 273A potentiostat was used in these measurements. The optical investigations were carried out at room temperature using a Shimadzu 3101 PC double-beam Spectrophotometer in the 320–3200 nm wavelength range.

3 RESULTS AND DISCUSSION

3.1 Structure and Morphology of the Films

Figure 1 shows the typical XRD spectra of V_2O_5 films spin-coated at 2400 rpm and annealed in air for 1 hour at 150, 200, 300 and 400 °C. The spectrum of the 150 °C annealed film shows a small and broadened peak at about $2\theta \approx 24°$. This peak can be attributed to (1 1 0) orthorhombic V_2O_5 lattice plane [4, 13]. After annealing in air at 300 and 400 °C, a new peak appears at $2\theta \approx 20°$ and the peak at $2\theta \approx 24°$ decreases in intensity and disappears after annealing at 400 °C. Another small peak can be observed around $2\theta \approx 40°$. These peaks are indexed assuming the orthorhombic symmetry. They are assigned to the (0 0 1) and (0 0 2) lattice planes showing that the structure of the films has a c-axis preferred orientation, the (0 0 1)-type planes lying parallel to the substrate. The same crystallographic structure was found for as-prepared V_2O_5 thin films grown by r.f. sputtering under a gas mixture of argon and oxygen [11], for spin-coated and heat-treated V_2O_5 films above 300 °C [5] and for sol–gel dip coating films pyrolyzed at 400 °C on a fused silica substrate [7]. The c-axis pre-ferred growth is also found for V_2O_5 films prepared by pulsed-laser deposition [14], by
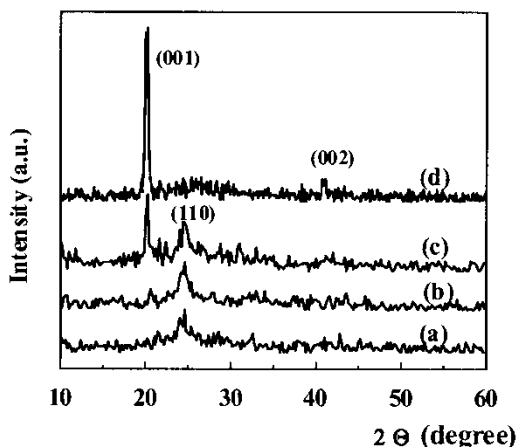
FIGURE 1   XRD spectra for sol–gel 2400 rpm spin-coated V$_2$O$_5$ thin films and annealed in air at: (a) 150 °C, (b) 200 °C, (c) 300 °C and (d) 400 °C.

plasma-enhanced chemical vapor deposition [15] and by vapor deposition in high vacuum [16] on heated substrates. Finally, other workers found that spin-coated V$_2$O$_5$ films were amorphous after annealing at a temperature of 300 °C for 1 hour. These films crystallize only after heat treatments at or above 380 °C [4].

The 150 °C annealed films' microstructure was analyzed by SEM. A typical surface micrograph is shown in Figure 2. It was found that the film surface was relatively smooth and neither cracks nor macroscopic porosity were observed at the used magnification. Further investigations on the microscopic structure must be made to conclude on the existence of porosity in the films (bulk density, pore size, . . .).

3.2   Thickness Profile

In this study, we have used the 1800 rpm spin-coated and 150 °C annealed films. These films were deposited on long substrates (5 cm) in order to investigate the centrifugal force effect on the film thickness profile. The samples are analyzed by optical transmission measurements on several substrate positions from one edge to the other. Thicknesses are calculated using the method described in Ref. [10].
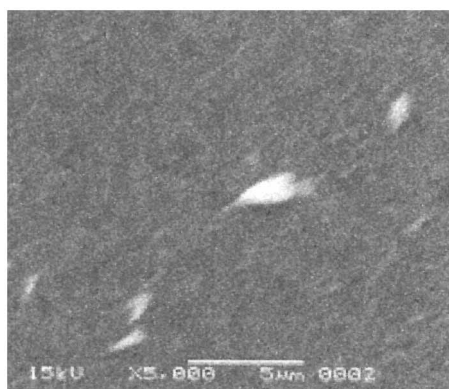

FIGURE 2   Typical SEM micrograph of 150 °C-dried sol–gel spin-coated V$_2$O$_5$ thin films.
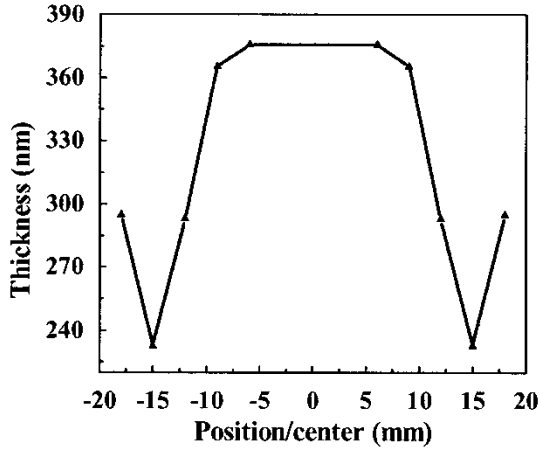
FIGURE 3   Thickness profile of spin-coated and $150\,^{\circ}$C annealed V_2O_5 thin films.

As illustrated in Figure 3, the film thickness is a maximum in the substrate center and decreases towards the substrate edge and then increases. The decrease is due to the fact that the centrifugal forces increase with the distance from the center of the substrate. At the edge of the substrate, a meniscus forms due to the surface tension at the edge [17]. This meniscus will restrict material flow and causes the thickness to increase at the edge.

3.3   Optical Properties

In order to calculate the optical and physical constants from the transmission spectrum only, the latter must contain more than three interference fringes [10]. As the number of fringes is a function of film thickness, and as the film thickness was found to increase when the spinning time and the spinning speed are decreased, we have used a speed of 1800 rpm to obtain a thicker film. A typical measured transmission spectrum $T(\lambda)$ of the $150\,^{\circ}$C treated films is shown in Figure 4. The envelope of the transmission curve in the oscillating region around
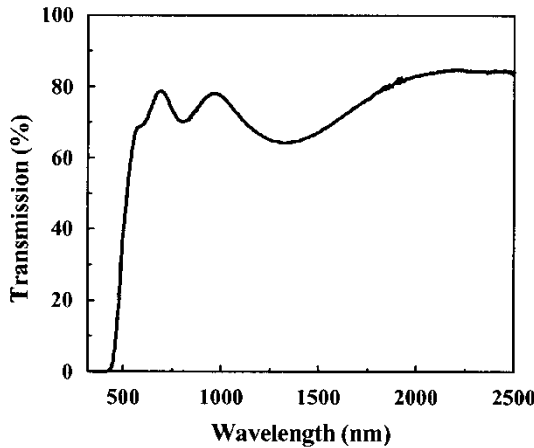

FIGURE 4   Transmission spectrum of V_2O_5 thin films spin-coated at 1800 rpm.

TABLE I   Results Obtained from the Optical Interference Method.

d (Å)	Δd (Å)	σ (Å)	n$_\infty$	b (μm)	λ_0 (μm)
4596	208	533	2.11	0.413	0.465

its extrema and the corresponding wavelengths (λ_{max} and λ_{min}) is used to calculate the refractive index n(λ). Then, film thickness and absorption coefficient are determined using a method, which takes into account the thickness inhomogeneity in the film [10].

Table I shows the results obtained assuming a thickness variation σ. Δd is the standard deviation of the calculated thickness, n$_\infty$, b, and λ_0 are the constants computed from the Sellmeir law fit [18]:

$$n^2(\lambda) = n_\infty^2 + \frac{b^2}{(\lambda^2 - \lambda_0^2)}$$

where n$_\infty$ is the IR extrapolated refractive index. The Sellmeir law accurately fits the experimental refractive index as it is shown in Figure 5 and gives an extrapolated refractive index to IR frequencies n$_\infty \approx 2.11$.

The absorption coefficient of the film is shown in Figure 6 and presents two distinct regions. The first one at h$v > 2.25$ eV can be fitted by Tauc's law [19]: $(\alpha h v) = A(h v - Eg)^2$, indicating that $(\alpha h v)^{1/2}$ varies linearly with hv in this region. This dependence is characteristic of an allowed indirect band-gap and the extrapolation of the $(\alpha h v)^{1/2}$ vs. (hv) to $\alpha = 0$ gives a band-gap Eg ≈ 2.3 eV (Fig. 7). The second region for h$v < 2.25$ eV is dominated by an exponential tail and is associated with transitions involving impurity states within the band-gap [20].

These results can be compared with our previous work on sputtered V$_2$O$_5$ thin films [11] and with other works [4, 21–28]. The optical transmission (Fig. 4) shows that spin-coated V$_2$O$_5$ thin films are weakly absorbing in the 550–2500 nm spectral range, with an absorption edge near 550 nm. These results are in accordance with those of sputtered V$_2$O$_5$ [11] and of electron beam evaporated [24] thin films (absorption edge in the 550–600 nm range). Other authors have reported the fundamental absorption edges in the 460–550 nm region [26–28], while Watanabe et al. have found an absorption edge near 400 nm for V$_2$O$_5$ thin films deposited by means of plasma MOCVD [25].
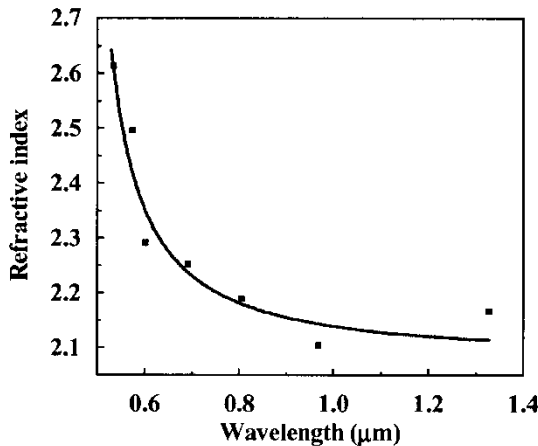
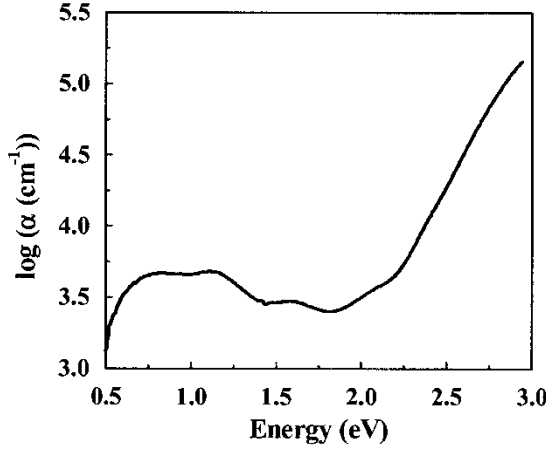FIGURE 5   Refractive index of V$_2$O$_5$ thin films spin-coated at 1800 rpm.

FIGURE 6   Absorption coefficient versus photon energy for V_2O_5 thin films spin-coated at 1800 rpm.

The $n_\infty \approx 2.11$ found in this work is close to that found for sputtered films (2.18 in Ref. 11). This value is however lower than that found by other authors for V_2O_5 sol–gel films (2.25 in Ref. 21) and for films prepared by means of plasma MOCVD (2.35 in Ref. 25). In other works, $n_\infty \approx 1.9$ for V_2O_5 films prepared by sol–gel spin-coating [4] and by electron beam evaporation [24] techniques. Such a lower value is taken as indicative of lower-density films which are required to produce a fast switching electrochromic coating [4].

The band-gap value 2.3 eV obtained here for spin-coated films is slightly greater than that obtained for sputtered and for V_2O_5 thin films prepared by means of plasma MOCVD (2.15 eV in Refs. 11 and 25). Other authors have reported that Eg changes from 2 eV to 2.38 eV [20–24, 26, 29]. It should be noted that the variation in the band-gap energy might be related to the degree of non-stoichiometry in V_2O_5 thin films [30].

The variation of the absorption coefficient (α) could not be fitted to a direct gap type law. It is found, however, that an indirect allowed gap ($(\alpha h\nu)^{1/2}$ linear with $h\nu$) yields a better fit. This is in good agreement with a theoretical band calculation [31] and with recent single
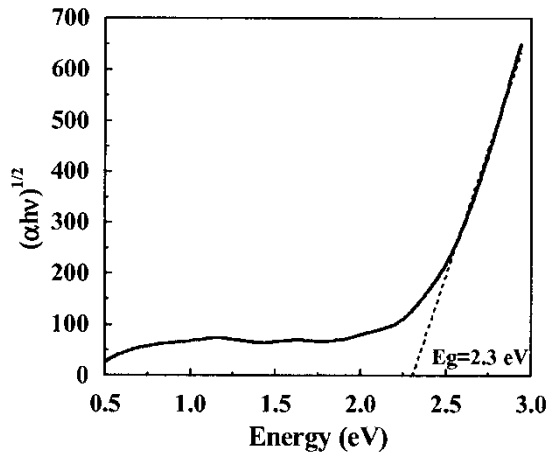

FIGURE 7   Fit of the absorption coefficient by Tauc's law.

crystal data [32]. However, this disagrees with band edge studies of V$_2$O$_5$ made by other authors [22–24, 28, 33] who suspected a direct forbidden band edge. Based on spectroscopic ellipsometry, other authors [15] have found that the absorption near the intrinsic edge cannot be described by a unique interband optical transition mechanism (allowed or forbidden, and direct or indirect transition). The authors explained this by the presence of nanocrystals dispersed in the amorphous matrix of the analyzed V$_2$O$_5$ films [15].

3.4 Electrochromic Properties

For these measurements, we have used V$_2$O$_5$ thin films spin-coated at 2400 rpm ($\sim$200 nm thick films) and annealed at 150 °C. Figure 8 shows the linear-sweep CV at various sweeping rates in the -0.4 V to $+1.2$ V (vs. SCE) potential range. The films gave excellent reversible CV with two-step electrochromism, i.e., yellow-orange to green, and green to blue. Two reduction/oxidation peaks can be observed. As reported in the literature, only a fraction of the V^{5+} ions are reduced to V^{4+} in the first reduction peak (peak A in Fig. 8) leading to a (V^{4+}, V^{5+}) mixture. The remaining V^{5+} ions are reduced to V^{4+} in a second step (peak B in Fig. 8). The same explanation is given for the two-oxidation pairs, i.e. the V^{4+} ions incomplete oxidation leaving a mixture of V^{4+} and V^{5+} (peak B$'$ in Fig. 8) and the oxidation of the remaining V^{4+} ions leading to V^{5+} ions (peak A$'$ in Fig. 8). Cogan et al. [28] has observed two such peaks and ascribed them to the formation of different crystalline phases of Li$_x$V$_2$O$_5$ upon the double injection/extraction of Li$^+$ and electron following the reaction equation [2, 34–36]:

$$V_2O_5 + xLi^+ + x\acute{e} \leftrightarrow Li_xV_2O_5.$$
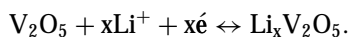
In the cathodic scan, the current density starts to increase substantially at potentials below $+0.6$ V and down to -0.3 V (curve e). Correspondingly, the film progressively loses its original yellow-orange color and becomes first green and then blue when the decreasing potential reaches -0.4 V. On the reverse scan, the oxidation peaks (B$'$ and A$'$) appear at 0.1 V and 0.75 V, respectively. At A$'$ the green color disappeared and the film regains its original yellow-orange color, indicating that both electrons and Li$^+$ ions were removed from the oxide framework under the anodic potential.
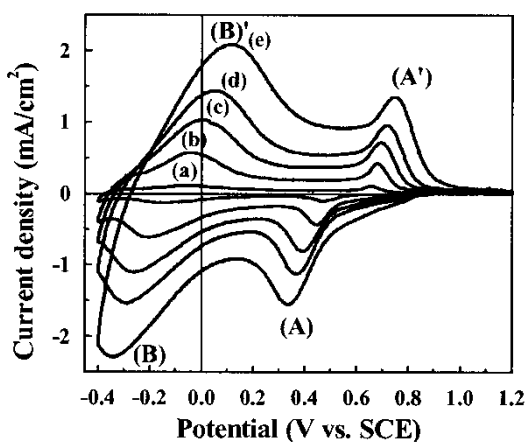

FIGURE 8   Cyclic voltammograms of 2400 rpm spin-coated V$_2$O$_5$ thin films at various sweeping rates: (a) 2 mV/s, (b) 10 mV/s, (c) 20 mV/s, (d) 30 mV/s and (e) 50 mV/s.

It should be noted finally that when the scan rate increases, the reduction peaks shift to more cathodic potentials while the oxidation peaks move to more anodic values suggesting that the electrochromism in V_2O_5 thin films is a slow process. Furthermore, the peak current densities increase with increasing sweeping rates showing that the process is controlled by the diffusion of Li^+ ions [4] as suggested by the linear dependence of the cathodic peak current densities (Ip_A and Ip_B) on the square root of the sweeping rate (Fig. 9). Other authors have found the same linear dependence of the cathodic peak current densities on the square root of the potential sweeping rate for high scan rates ($v > 0.5$ mV/s) [37] suggesting that a semi-infinite linear diffusion transport within the film controls the current response. Furthermore, for scan rates slower than 0.1 mV/s, the authors have found a linear dependence of the peak current density on the polarization scan rates [37]. Some authors [38, 39] have used the potentiostatic intermittent titration (PITT) and electrochemical impedance spectroscopy (EIS) to explore Li ion intercalation into thin V_2O_5 electrodes and have applied the finite diffusion models for the interpretation of their results. Details on the intervening processes during lithium intercalation in our sol–gel spin-coated V_2O_5 thin films are under investigation using impedance spectroscopy.

The transients' behavior of the coloration–decoloration process was further investigated using the chronoamperometry technique. The 150 °C annealed film was biased for 15 min at a cathodic potential of −400 mV (blue color). This is followed by an anodic potential of 1200 mV for an equal time to bleach the film to its initial color (yellow-orange). For both steps, the current density was measured as a function of the coloration and decoloration time (Fig. 10(a) and 10(b), respectively). As can be seen, the coloration and the decoloration need ∼100 s to be complete. In other works, the coloration needs more time than the bleaching [12, 40]. A pronounced hysteresis has been observed in the lithium intercalation/deintercalation behavior for a set of tungsten oxide-based electrochromic devices [41]. The time for the coloration to be complete (100 s) is lower than that found for sputtered V_2O_5 thin films (150 s in Ref. 12). This indicates that V_2O_5 films prepared by the sol–gel process are suitable as a fast switching electrochromic coating.

Finally, the peaks observed in CV measurements for our spin-coated thin films are much better resolved than those obtained with the sputtered V_2O_5 thin films [12] and with spin-coated V_2O_5 thin films deposited by the same route [1]. On the other hand, the potential separation of the two consecutive oxidation or reduction peaks for spin-coated films found
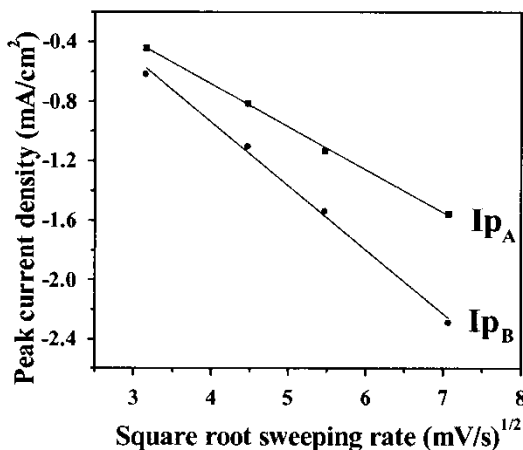

FIGURE 9   Peak current densities versus square root sweeping rates. (Ip_A): first reduction peak, (Ip_B): second reduction peak.
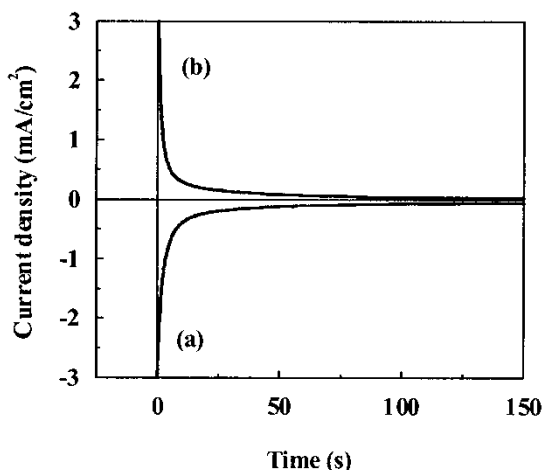
FIGURE 10 Current density during coloration at −400 mV (a) and bleaching at 1200 mV (b) for 15 min.

here is higher than that found for sputtered films (0.65 V compared to 0.3 V for sputtered films [12] at a 50 mV/s sweeping rate). Levi et al. [42] have observed the same behavior on evaporated V$_2$O$_5$ thin films deposited on two different substrates and have attributed the pronounced difference between the two peak potentials to a different degree of crystallization of the films. Other works [43] made on V$_2$O$_5$ xerogel have shown that the lithium insertion into the xerogel gives rise to only one step located around 3.1 V (vs. Li/Li$^+$). This may correspond to a poor separation between the two consecutive intercalation stages. The same behavior has been observed for V$_2$O$_5$ films deposited by the sol–gel dip coating technique, the films showed then one step electrochromism yellowish to greenish on the oxidized and reduced state, respectively [44].

The transmission spectra of the as-deposited and annealed at 150 °C, colored to green at +200 mV, to blue at −400 mV and of bleached films at +1200 mV vs. SCE for 15 min are shown in Figure 11. The blue colored films have a 30% transmission in the visible region (Fig. 11(d)), while the as-deposited films reached 80% in the same wavelength range
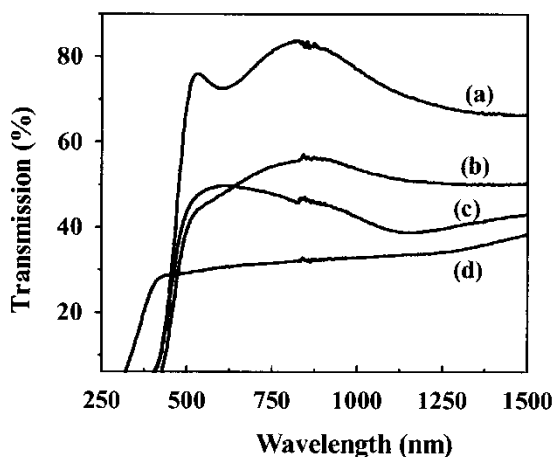

FIGURE 11 Transmission spectra of spin coated V$_2$O$_5$ thin films treated at various applied potentials: (a) as-deposited, (b) +1200 mV, (c) +200 mV and (d) −400 mV.
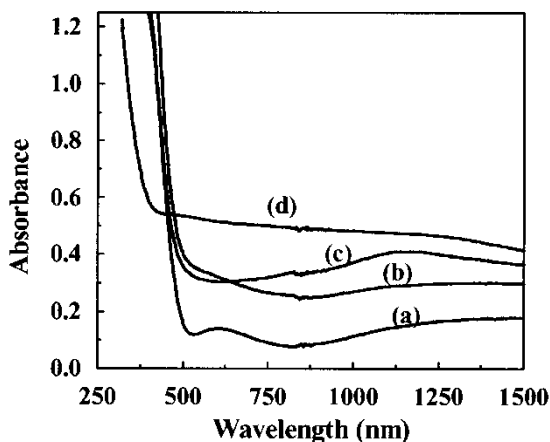
FIGURE 12   Absorption spectra of spin-coated V_2O_5 thin films treated at various applied potentials: (a) as-deposited, (b) +1200 mV, (c) +200 mV and (d) −400 mV.

(Fig. 11(a)). When bleached, the film transmission (Fig. 11(b)) does not come back to its initial value suggesting that after bleaching some Li^+ ions are still in the V_2O_5 matrix [45]. The film transparency found here (80%) for as-deposited films is in agreement with that found for sol–gel dip coating V_2O_5 thin films [44]. However, this transparency is larger than that (60%) found for as-prepared two-spin sol–gel films [1]. This difference cannot be attributed to a film thickness as we have found the same transmission value (80%) in the VIS–PIR wavelength range for two different thickness V_2O_5 films (∼4600 Å in Sec. 3.3 and ∼2000 Å in this section). This may be due, in contrast, to a difference in the refractive index and absorption coefficient. This later is probably due to annealing twice (heat treatment after each spin-coating) for the two-spin film in Ref. [1] leading to more absorbing films. Another explanation may be the increased reflection losses due to the fact that in Ref. [1] two layers were deposited instead of a single layer.

On the other hand, the transmittance change found here for the film between the colored and the bleached states for wavelengths larger than 500 nm ($\Delta T = 25\%$) is less than that found by the authors ($\Delta T = 40\%$) in Ref. [1] for the two-spin film. This transmittance change is fortunately higher than that found for sol–gel dip-coating [44, 45] and sol–gel spin-coating [4] V_2O_5 films ($\Delta T_{vis} = 20\%$, 10% and 13% in Refs. 44, 45 and 4, respectively).

The corresponding absorption spectra in the 250–1500 nm wavelength range are presented in Figure 12. When polarized at −400 mV (Fig. 12(d)), the film gives a strong optical absorption in the $\lambda > 500$ nm range. When a more anodic potentials are applied (Fig. 12(c) and 12(b)), the absorption in the same wavelength range decreases but does not reach the absorbance of the as-deposited film (Fig. 12(a)), while the optical absorption edge shifts to lower energies. So, intercalation of Li^+ ions into the V_2O_5 matrix increases the optical gap. This band-gap widening upon increased Li content is in agreement with earlier results on nano-crystalline $Li_xV_2O_5$ films produced by sputtering [46], but does not agree with those on polycrystalline $Li_xV_2O_5$ [46] and on some work on V_2O_5 gel layers [47].
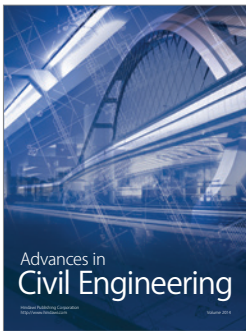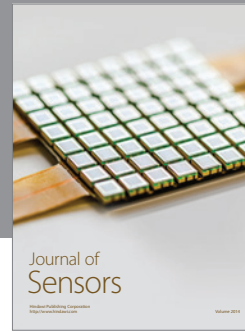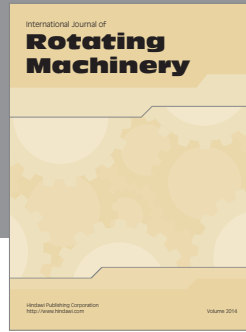
4 CONCLUSION

In this work, we have presented structural, optical and electrochemical studies of V_2O_5 thin films prepared by the sol–gel spin-coating method. The polycrystalline nature of the resulting

V$_2$O$_5$ thin films has been shown and a c-axis preferred orientation was found after annealing in air at 400 °C. The theoretical idea for the thickness increasing in the sample edges (edge bead) for the spin-coating method is confirmed experimentally by calculating the thickness profile. Furthermore, we have calculated the optical constants as well as the thickness variation σ (thickness inhomogeneity) using the transmission spectrum alone. We have shown, on one hand, that the films have very acceptable optical properties with a clear low absorption region, a high transparency (80%), a relatively low refractive index n$_\infty$ and a large band-gap. On the other hand, these films gave excellent reversible electrochromism with two coloration steps: yellow-orange $\leftrightarrow$ green $\leftrightarrow$ blue. The cyclic voltammograms are found to be well resolved and the changes in color have been explained by the progressive pentavalent/tetravalent V ions reduction/oxidation by the double injection/extraction of electrons and Li$^+$ ions into/from the V$_2$O$_5$ matrix. At the same time, the colored films gave a strong optical absorption in the range $\lambda > 500$ nm and a higher optical gap as compared with the as-deposited or bleached films. The coloration and the decoloration need moderate time to be complete, so the V$_2$O$_5$ films prepared by the sol–gel process are suitable as a fast switching electrochromic coating.

References

[1] Zhongchun Wang, Jiefeng Chen and Xingfang Hu. (2000). Thin Solid Films, 375, 238.
[2] Granqvist, C. G. (1995). In: Handbook of Inorganic Electrochromic Materials. Elsevier, Amsterdam, p. 295.
[3] Özer, N. and Lampert, C. M. (1999). Thin Solid Films, 349, 205.
[4] Özer, N. (1997). Thin Solid Films, 305, 80.
[5] Youichi Shimizu, Katsumi Nagase, Norio Miura and Noboru Yamazoe. (1990). Jap. J. Appl. Phys., 29, L1708.
[6] Katsumi Nagase, Youichi Shimizu, Norio Miura and Noboru Yamazoe. (1992). Appl. Phys. Lett., 60, 802.
[7] Partlow, D. P., Gurkovich, S. R., Radford, K. C. and Denes, L. J. (1991). J. Appl. Phys., 70, 443.
[8] Hiroshi Hirashima and Kazumi Sudoh. (1992). J. Non-Cryst. Solids, 145, 51.
[9] El Mandouh, Z. S. and Selim, M. S. (2000). Thin Solid Films, 371, 259.
[10] Bennouna, A., Laaziz, Y. and Idrissi, M. A. (1992). Thin Solid Films, 213, 55.
[11] Benmoussa, M., Ibnouelghazi, E., Bennouna, A. and Ameziane, E. L. (1995). Thin Solid Films, 265, 22.
[12] Benmoussa, M., Outzourhit, A., Bennouna, A. and Ameziane, E. L. (2002). Thin Solid Films, 405, 11.
[13] ASTM Powder Diffraction Data Cards, International Center for Diffraction Data, New York 1983, Cards 9–387.
[14] Julien, C., Haro-Poniatowski, E., Camacho-Lopez, M. A., Escobar-Alarcon, L. and Jimenez-Jarquin, J. (1999). Materials Science and Engineering, B65, 170.
[15] Losurdo, M., Barreca, D., Bruno, G. and Tondello, E. (2001). Thin Solid Films, 384, 58.
[16] AboElSoud, A. M., Mansour, B. and Soliman, L. I. (1994). Thin Solid Films, 247, 140.
[17] Jeffreg Taylor, F., Ph. D. Sony Chemicals Corporation of America, 1001 Technology Drive, Mt. Pleasant, PA 15666.
[18] Bruhat, G. (1959). In: Kastler, A. (Ed.), Cours de Physique Générale-Optique, 5th ed. Masson & Cie, Paris, p. 372.
[19] Tauc, J. (1972). In: Optical Properties of Solids. North-Holland, Amsterdam, p. 277.
[20] Aita, C. R., Ying-Liliu, MeiLee Kao and Hansen, S. D. (1986). J. Appl. Phys., 60, 749.
[21] Rubin, M., Von Rottkay, K., Wen, S.-J., Ozer, N. and Slack, J. (1998). Solar Energy Materials and Solar Cells, 54, 49.
[22] Madhuri, K. V., Naidu, B. S., Hussain, O. M., Eddrief, M. and Julien, C. (2001). Materials Sciences and Engineering B, 86, 165.
[23] Ramana, C. V., Hussain, O. M., Srinivasulu Naidu, B., Julien, C. and Balkanski, M. (1998). Materials Sciences and Engineering B, 52, 32.
[24] Ramana, C. V., Hussain, O. M., Uthanna, S. and Srinivasulu Naidu, B. (1998). Optical Materials, 10, 101.
[25] Hideto Watanabe, Ken-ichi Itoh and Osamu Matsumoto. (2001). Thin Solid Films, 386, 281.
[26] Kenny, N., Kannewurf, C. R. and Whitmore, D. H. (1966). J. Phys. Chem. Solids, 27, 1237.
[27] Clauws, P. and Vennik, J. (1974). Phys. Status Solidi B, 66, 553.
[28] Cogan, S. F., Nguyen, N. M., Perrotti, S. J. and Rauh, R. D. (1989). J. Appl. Phys., 66, 1333.
[29] Moshfegh John Luksich, A. Z. and Carolyn Rubin Aita. (1991). J. Vac. Sci. Technol., A9, 542.
[30] Moshfegh, A. Z. and Ignatiev, A. (1991). Thin Solid Films, 198, 251.
[31] Lambrecht, W., Djafari-Rouhani, B., Lannoo, M. and Vennik, J. (1980). J. Phys. C: Solid State Phys., 13, 2485.
[32] Parker, C. R., Lam, D. J., Xu, Y.-N. and Ching, W. Y. (1990). Phys. Rev. B, 42, 5289.
[33] Bodo, Z. and Hevesi, I. (1967). Phys. Status Solidi, 20, K45.
[34] Talledo, A. and Granqvist, C. G. (1995). J. Appl. Phys., 77, 4655.
[35] Wang, Z.-C., Chen, X.-F., Li, Z.-Y. and Hu, X.-F. (1999). Chin. J. Ceramic Soc., 27, 28.

[36] Wang, Z.-C., Li, Z.-Y., Chen, X.-F. and Hu, X.-F. (1999). Acta Phys. Sin., 8, 57.
[37] Krtil, P. and Fattakhova, D. (2001). J. Electrochem. Soc., 148, A1045.
[38] Levi, M. D., Lu, Z. and Aurbach, D. (2001). Solid State Ionics, 143, 309.
[39] Lu, Z., Levi, M. D., Salitra, G., Gofer, Y., Levi, E. and Aurbach, D. (2000). J. Electroanal. Chem., 491, 211.
[40] Fujita, Y., Miyazaki, K. and Tatsuyama, C. (1985). Jpn. J. Appl. Phys., 24, 1082.
[41] Denesuk, M., Cronin, J. P., Kennedy, S. R. and Uhlmann, D. R. (1997). J. Electrochem. Soc., 144, 1971.
[42] Levi, M. D., Zhonghua Lu, Gofer, Y., Yaron Cohen, Yair Cohen, Aurbach, D., Vieil, E. and Serose, J. (1999). J. Electroanal. Chem., 479, 12.
[43] Pereira-Ramos, J. P., Baddour, R., Bach, S. and Baffier, N. (1992). Solid State Ionics, 53–56, 701.
[44] Özer, N., Sabuncu, S. and Cronin, J. (1999). Thin Solid Films, 338, 201.
[45] Crnjak Orel, Z. and Musevic, I. (1999). NanoStructured Materials, 12, 399.
[46] Talledo, A., Anderson, A. M. and Granqvist, C. G. (1991). J. Appl. Phys., 69, 3261.
[47] Bullot, J., Cordier, P., Gallais, O., Gauthier, M. and Baborneau, F. (1984). J. Non-Cryst. Solids, 68, 135.